

## PHASE EFFECT ON DEFORMATION ANISOTROPY OF STRENGTH AND FRACTURE RESISTANCE CHARACTERISTICS OF TITANIUM ALLOYS

S. B. Nizhnik and E. A. Dmitrieva

UDC 539.37:669.15

*Comparative analysis of anisotropy of mechanical characteristics of titanium and aluminum alloys as well as austenitic steel in the formation of structural and crystallographic texture on rolling and in biaxial tension was carried out. The effect of increasing the  $\beta$ -phase content in titanium alloys on the suppression rate of “reverse anisotropy” of fracture resistance and texture strengthening was examined. The mechanisms of a similar strengthening effect of a plane stress state on the plastic deformation resistance of  $\alpha$ -titanium alloys and austenitic steel with the metastable structure were discussed.*

**Keywords:** titanium and aluminum alloys, metastable austenitic steel, anisotropy of mechanical characteristics, structural and crystallographic sheet texture, biaxial tension.

**Introduction.** One of the lines of research for optimizing anisotropy of mechanical characteristics of structural metals in service is to elucidate the effect of material structure inhomogeneity patterns on plastic deformation and fracture resistance. The notion “structure inhomogeneity” as applied to rolled metals includes phase composition, structural texture, and different types of strain-induced crystallographic texture.

The structural texture accounts for a directional change in the form, size, and orientation of grains and subgrains of matrix phases on rolling, for ageing alloys, it is also change in the distribution density of dispersion particles of strengthening phases along the boundaries of structure elements. Such a texture exerts decisive influence on the anisotropy of mechanical properties of metals with fcc and bcc lattices having a large number of active slip systems.

The crystallographic texture is representative of the preferred orientation of crystallites, limiting the number of active slip planes in certain crack propagation directions, and thus, the ability of the material to evolve the plastic zone near its tip in those directions, which involves a corresponding change in fracture toughness. The effect of crystallographic texture of the material on the anisotropy of its fracture toughness is greatly enhanced for the metals and alloys with the hcp lattice of the matrix phase, possessing a much smaller number of active slip systems as compared to the metals with the fcc and bcc lattices.

Combined effects of the above structure inhomogeneity on the anisotropy of fracture resistance characteristics are as yet imperfectly understood. It prevents from establishing general patterns of its behavior with regard to an alloying technique, plastic prestrain level, and thermal treatment method, influencing the phase composition of the material and its structural and crystallographic texture. The latter is especially topical for a wide range of multiphase titanium alloys, exhibiting simultaneously the crystallographic and structural texture of a rolled metal. The extent of their interaction is dependent on the quantitative ratio of the  $\alpha$ - and  $\beta$ -phases with the hcp and bcc lattices, respectively.

As the advancement of investigations performed for  $\alpha$ - and pseudo- $\alpha$ -titanium alloys [1], this study is devoted to analysis and systemization of experimental data for initially duplex titanium alloys, deformed under a

---

Timoshenko Institute of Mechanics, National Academy of Sciences of Ukraine, Kiev, Ukraine (fract@imech.kiev.ua). Translated from Problemy Prochnosti, No. 6, pp. 81 – 92, November – December, 2014. Original article submitted September 22, 2014.

TABLE 1. Examined Alloys and Their Classification by the Phase Composition

No.	Alloy	[Al] <sub>eq</sub> , %	[Mo] <sub>eq</sub> , %	Phase composition
1	VT1-0	1.2	0	α-Alloys
2	VT5-1	6.8	0	
3	OT4-1	2.5	1.7	Pseudo-α-alloys
4	VT20	7.8	1.7	
5	OT4	5.0	2.5	
6	VT6	7.0	3.2	(α + β)-Alloys
7	VT8	7.5	3.3	
8	VT9	7.7	3.4	
9	VT14	6.0	4.0	
10	VT3-1	7.3	6.3	
11	VT23	6.5	8.4	
12	VT16	4.0	8.2	
13	VT30	3.5	11.5	Intermediate-structure alloys
14	VT22	6.0	12.7	
15	VT15	4.0	25.3	Pseudo-β-alloy

competing influence of the crystallographic and structural texture of a rolled metal on the anisotropy of strength, plasticity, and fracture resistance characteristics with regard to a stress state [2–4]. The anisotropy of mechanical properties on combined and separate texture and structure strengthening of those metals was compared with the results, obtained earlier for α-titanium and aluminum alloys as well as for austenitic stainless steel on rolling, in uni- and biaxial tension [1, 5–10].

**1. Objects of Investigation and Basic Deformation Anisotropy Characteristics.** Classification of titanium alloys by their phase composition is given in Table 1, it includes α- and pseudo-α-alloys, (α + β)-alloys, intermediate-structure alloys, and a pseudo-β-alloy. They are directionally alloyed as evidenced by generalized characteristics of the chemical composition, viz aluminum [Al]<sub>eq</sub> and molybdenum [Mo]<sub>eq</sub> equivalents, including a series of alloying elements that stabilize the α- and β-phases, respectively [2]

$$[\text{Al}]_{eq}, \% = \% \text{Al} + \% \text{Sn}/3 + \% \text{Zn}/6 + 10[\% \text{O} + \% \text{C} + 2(\% \text{N})], \quad (1)$$

$$[\text{Mo}]_{eq}, \% = \% \text{Mo} + \% \text{Ta}/4 + \% \text{Nb}/3.3 + \% \text{W}/2 + \% \text{V}/1.4 + \% \text{Cr}/0.6 + \% \text{Nb}/0.8 + \% \text{Mn}/0.6 + \% \text{Fe}/0.4. \quad (2)$$

Diagrams of the phase composition of titanium alloys after process annealing, when the quantitative ratio of the α- and β-phases close to the equilibrium one is observed [2], were used to graphically represent the most probable content of the β-phase  $f_\beta$  vs [Mo]<sub>eq</sub> in examined alloys (Fig. 1).

Titanium alloys were analyzed using 57-mm thick plates (VT6 alloy) with the perfect texture of the α-phase of edge type and sheets (2–3 mm) of several alloys with the basic texture of the α-phase of central type, formed under deformation with the total reduction to  $\varepsilon = 0.8\text{--}0.85$  (Table 1).

In the general case (for thin plates), correlating fracture resistance characteristics [3], viz the critical stress intensity factor  $(K_{Ic})_{MN}$  (fracture toughness) and work of fracture  $(KCV)_{MN}$ , were determined on the specimens of  $MN = 12, 21, 13, 31, 23,$  and  $32$  type cut from a rolled object according to the scheme in Fig. 2a [1, 4, 11]. For the examined characteristics,  $M = 1, 2,$  and  $3$  represents longitudinal (rolling direction), transverse, and normal (to the rolling plane) directions of active force, respectively,  $N = m$  denotes the mode I crack propagation direction in the corresponding plane  $(mn) = (23), (13), (32), (12), (31),$  and  $(21)$ .

The scheme of a structurally textured aluminum alloy fragment with the pronounced nonequiaxiality of matrix phase grains, determined by the size  $d_M$ –direction  $M$  ( $d_1 > d_2 > d_3$ ) relation, is presented in Fig. 2b.

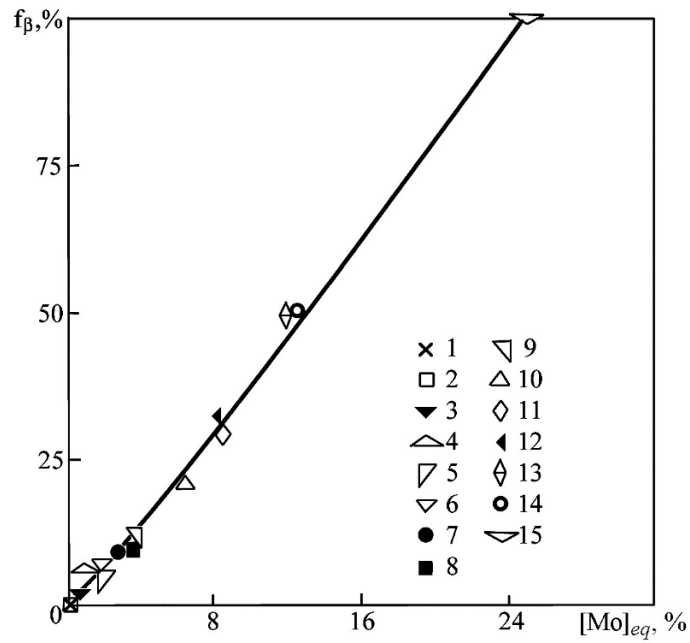


Fig. 1. The  $\beta$ -phase content in titanium alloys vs their chemical composition characteristic  $[Mo]_{eq}$ . (Symbols according to alloy numbering in Table 1).

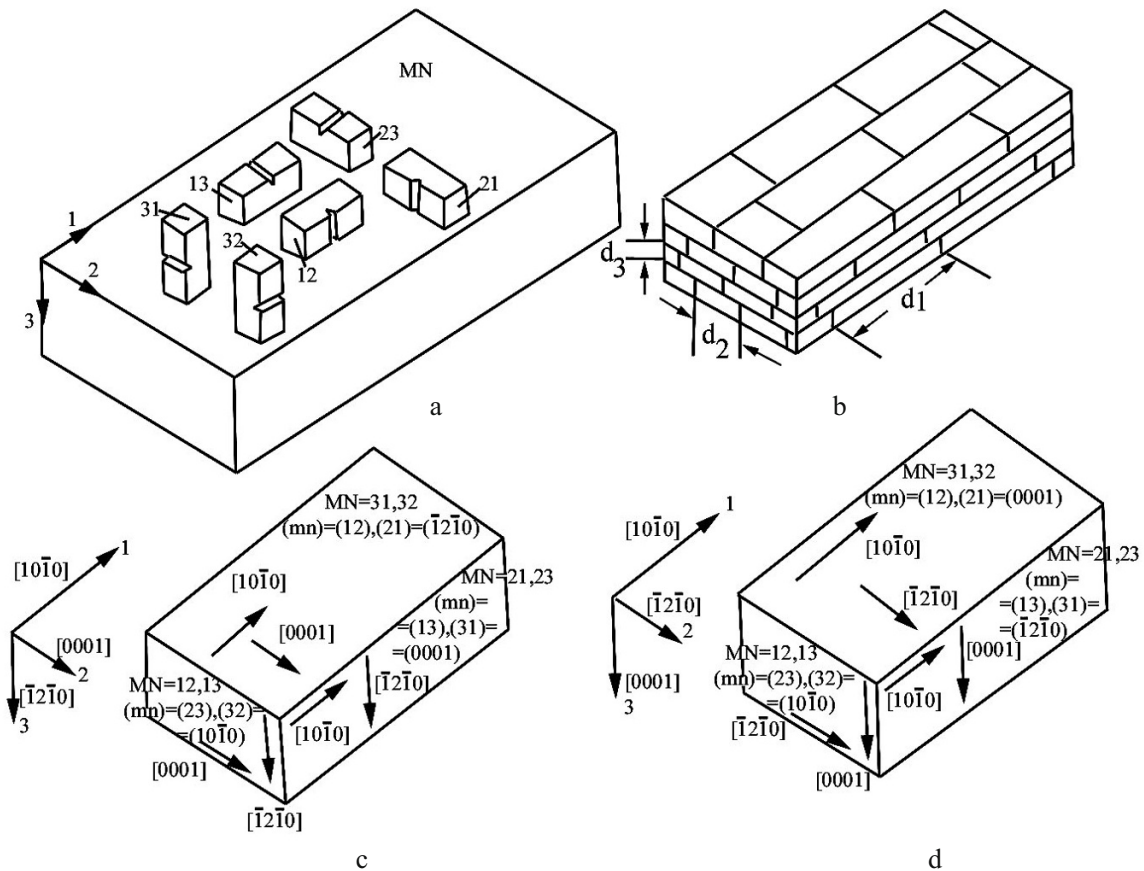


Fig. 2. Schemes of specimen cutting from a rolled plate for estimating fracture resistance characteristics (a), specimen fragments with the structural (b) and crystallographic texture of types I (c) and II (d) with indication of prismatic slip systems.

The scheme of a thick plate fragment from a titanium alloy with the perfect crystallographic texture of edge type I after rolling and annealing is depicted in Fig. 2c. For such a texture, the basic plane  $(mn) = (hkl) = (0001)$  is normal to the rolling plane  $(hkl) = (\bar{1}2\bar{1}0)$  and parallel to the rolling direction  $M = 1 = [HKIL] = [10\bar{1}0]$  with the transverse direction  $M = 2 = [000\bar{1}]$  and the normal to the rolling plane  $M = 3 = [HKIL] = [\bar{1}2\bar{1}0]$ .

The scheme of a thin plate fragment from a titanium alloy with the perfect basic texture of central type II is shown in Fig. 2d. For such a texture, the basic plane  $(mn) = (hkl) = (0001)$  is parallel to the rolling plane and the rolling direction  $M = 1 = [HKIL] = [10\bar{1}0]$  with the transverse direction  $M = 2 = [HKIL] = [\bar{1}2\bar{1}0]$  and the normal to the rolling plane  $M = 3 = [HKIL] = [0001]$ . For illustration, nominal crystallographic orientations of the prismatic slip systems  $(hkl)[HKIL]$  are indicated in Fig. 2c, d.

The engineering yield stress  $(\sigma_Y)_M = (\sigma_{0.2})_M$  of the material was determined on standard crack-free specimens cut out in the directions  $M = 1, 2,$  and  $3$ .

For comparing the results of studying the strength and fracture resistance characteristics of thick and thin plates, this investigation was restricted to analysis of the specimens  $MN = 12$  and  $21$ .

A plane stress state in titanium alloys was accomplished on original plane U-notched specimens subject to plastic deformation in symmetrical biaxial tension  $\sigma_1/\sigma_2 = 1$  [3]. The effect of the plane stress state on the mechanical characteristics of stable and metastable austenitic steel was estimated with thin-walled tubular specimens subject to plastic deformation at  $20$  and  $-160^\circ\text{C}$  under the simultaneous action of tensile force and internal pressure at the ratio of principal stress components in the longitudinal ( $z$ ) and transverse ( $\theta$ ) directions  $\sigma_z/\sigma_\theta = \infty$  (uniaxial tension) and  $\sigma_z/\sigma_\theta = 1$  (equiaxial tension) [7–10].

**2. Results and Discussion.** The anisotropy formation mechanisms of strength and fracture resistance characteristics of single-phase and duplex titanium alloys were consistently analyzed considering the crystallographic texture of the  $\alpha$ -phase, as the  $\beta$ -phase content was directionally increased with  $[\text{Mo}]_{eq}$ . Examination was performed of the rolling effect of plastic strain levels on the crystallographic  $\alpha$ -phase texture, responsible for the deformation anisotropy, typical of hcp metals that is associated with the evolution of “reverse” anisotropy of strength and fracture resistance characteristics as well as texture strengthening at the plane stress state. An estimate was made of the function of the  $\beta$ -phase content in the above anisotropy. Discussion was devoted to the structural sources of its leveling in aluminum alloys and austenitic steel as well as the conditions of its possible evolution in the latter.

**2.1. Reverse Anisotropy of Strength and Fracture Resistance Characteristics vs Crystallographic Texture and Quantitative Ratio of Phases.** Reverse anisotropy is an enhanced ability of the material to retard plastic deformation and fracture resistance along the rolling direction (specimens  $MN = 21$ ) as compared to the transverse direction (specimens  $MN = 12$ ) that is mainly observed for hcp metals and is not exhibited by the metals with the fcc and bcc lattices. The structural texture of a rolled metal typical of the latter (Fig. 2b), examined with aluminum alloys, leads to a decrease in the strength ( $\sigma_Y$ ) and fracture toughness ( $K_{1c}$ ) characteristics in going from  $MN = 12$  specimens to  $MN = 21$  ones (Table 2, Fig. 3a). A decrease in the fracture toughness anisotropy characteristic  $A_{K_{1c}} = (K_{1c})_{21}/(K_{1c})_{12}$  with the strain  $\epsilon$ , as the loading direction changes from the longitudinal to transverse one [1, 5, 6], is the result of smaller numerical values of the fracture toughness  $(K_{1c})_{21}$  with an increase in the structural parameter of embrittlement, viz. the grain size  $d_1$  in the direction  $M = 1$ , and thus, the growth of anisotropy  $d_1/d_2$  under the change in  $(mn)$  from (23) to (13) (Fig. 3a).

The latter leads to a simultaneous decrease in the strength characteristic  $(\sigma_Y)_2$  as compared to  $(\sigma_Y)_1$ , which is well seen with a 7075 alloy (Table 2). With this, the change in the fracture mechanism from mostly plastic over the grain bodies to quasibrittle along their boundaries is quite possible. This probability becomes even higher under the intensification of grain-boundary segregation of strengthening phase particles, which increases the tendency of the material to intergranular fracture and rises its cold-brittleness temperature up to the test temperature of  $20^\circ\text{C}$  [5, 6, 12]. The reverse anisotropy of hcp metals is illustrated with  $\alpha$ - and pseudo- $\alpha$ -titanium alloys (Table 2), which were detailed earlier [1, 6].

As is seen from the data in Table 2, thick plates as compared to the thin ones exhibit smaller  $KCV$  values, which can be explained [1] by the change in the crack propagation mechanism, from twinning to prismatic and

TABLE 2. Strength ( $\sigma_Y$ ) and Fracture Resistance  $(K_{1c})_{MN}$ ,  $(KCV)_{MN}$  Characteristics of Sheets from Aluminum (7075) and Titanium (VT6, VT5-1, and OT4) Alloys vs Loading Direction and Nominal Slip Systems

A. Thick plates				
Alloy	7075		VT6	
Texture	Structural: $d_1 > d_2 > d_3$		Crystallographic I	
Loading direction $M$	1	2	$M - [HKIL]$	
			$1 - [10\bar{1}0]$	$2 - [0001]$
$(\sigma_Y)_M$ , MPa	482	466	929	1009
Orientation of specimens $MN(mm)$	12(23)	21(13)	12(23)	21(13)
	$(mn)/MN - (hkl)/[HKIL]$			
			$(10\bar{1}0)/[0001]$	$(0001)/[10\bar{1}0]$
$(K_{1c})_{MN}$ , $\text{MPa} \cdot \text{m}^{1/2}$	56,1	42,7	50.0	46.3
$(KCV)_{MN}$ , $\text{MJ/m}^2$	–	–	0.18	0.19
B. Thin plates				
Alloy	VT5-1		OT4	
Texture	Crystallographic II			
Loading direction $M$	$M - [HKIL]$			
	$1 - [10\bar{1}0]$	$2 - [\bar{1}2\bar{1}0]$	$1 - [10\bar{1}0]$	$2 - [\bar{1}2\bar{1}0]$
$(\sigma_Y)_M$ , MPa	630	750	662	765
Orientation of specimens $MN(mm)$	12(23)	21(13)	12(23)	21(13)
	$(mn)/MN - (hkl)/[HKIL]$			
	$(10\bar{1}0)/[\bar{1}2\bar{1}0]$	$(\bar{1}2\bar{1}0)/[10\bar{1}0]$	$(10\bar{1}0)/[\bar{1}2\bar{1}0]$	$(\bar{1}2\bar{1}0)/[10\bar{1}0]$
$(KCV)_{MN}$ , $\text{MJ/m}^2$	0.54	1.35	0.42	1.01

pyramidal slip in accordance with the change in nominal crystallographic crack propagation systems, from  $(10\bar{1}0)[1000]_{12}$ ,  $(1000)[10\bar{1}0]_{21}$  to  $(10\bar{1}0)[\bar{1}2\bar{1}0]_{12}$ ,  $(\bar{1}2\bar{1}0)[10\bar{1}0]_{21}$ . The change in this mechanism can be associated with the evolution of the crystallographic texture of type I to the texture of type II (Fig. 2c, d). The crystallographic systems, most favorable for prismatic and pyramidal slip,  $(10\bar{1}0)[\bar{1}2\bar{1}0]$ ,  $(0001)[\bar{1}2\bar{1}0]$ , and  $(10\bar{1}1)[\bar{1}2\bar{1}0]$  direct the basic plane  $(0001)$  parallel to the rolling plane and the slip vector  $[\bar{1}2\bar{1}0]$  to the basic plane (Fig. 2c, d) in accordance with a decrease in the relative atomic packing density of the above planes from 1.092 to 1.000 and 0.959 [13].

As is seen in Fig. 3b, an enhancement of the reverse anisotropy effect of  $KCV$  [ $A_{KCV} = (KCV)_{21}/(KCV)_{12}$ ] in going from thick to thin plates of an  $\alpha$ -titanium alloy can be connected with the formation of the basic texture of distorted type in such a way that the plane  $(10\bar{1}0)$  becomes more favorably oriented for the fracture resistance of specimens ( $MN = 21$ ) in the transverse direction as compared to ( $MN = 12$ ) in the longitudinal one [3, 4]. The latter results in a more pronounced reverse anisotropy for thin plates, while for thick plates, cross slip is effected over the planes  $(0001)$ .

For estimating the function of the  $\beta$ -phase content in the formation of the reverse anisotropy of fracture resistance characteristics, examined duplex alloys were compared at approximately constant aluminum equivalent values ( $[Al]_{eq} = 6.0\text{--}6.8$ ), determining the alloying extent of the  $\alpha$ -phase and influencing its crystallographic texture [3].

The pattern of reverse anisotropy characteristic ( $A_{KCV}$ ) variation with the  $\beta$ -phase content  $f_\beta$  in going from a VT5-1 alloy to OT4, VT14, VT30, VT22, and VT15 alloys (Table 1, Fig. 1) can be followed from the data in Fig. 3b, c, both under plastic deformation to  $\varepsilon = 0.8$  (sheet thinning from 6 to 2 mm) and with a directional increase

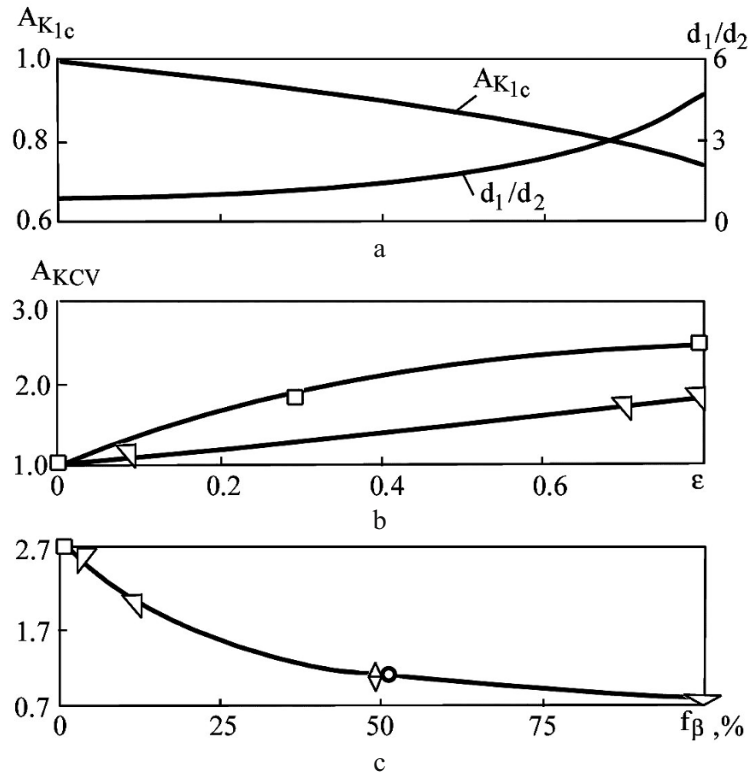


Fig. 3. Anisotropy of the structure parameters and fracture resistance characteristics of aluminum (a) and titanium (b, c) alloys vs strain  $\varepsilon$  on rolling (a, b) and  $\beta$ -phase content at  $\varepsilon=0.8$  (c). (Symbols for titanium alloys in Fig. 1 and Table 1).

in  $f_\beta$  over the whole range of its values for the alloys initially deformed to  $\varepsilon=0.8$ . As is seen, with an increase in the content of  $\beta$ -phase grains elongated in the rolling direction, the reverse anisotropy characteristic  $A_{KCV}$  smoothly decreases (2.7–0.7). At  $f_\beta < 50\%$ ,  $A_{KCV} > 1$ , which is caused by a prevailing influence of the crystallographic  $\alpha$ -phase texture of thin plates on the reverse anisotropy  $KCV$ . At  $f_\beta = 50\%$ , the above influence of the  $\alpha$ -phase texture and deformation anisotropy of the structural  $\beta$ -phase parameters on  $A_{KCV}$  is balanced, and the isotropic state of alloys is reached ( $A_{KCV} = 1$ ). A further growth of  $f_\beta$  leads to the change in the formation mechanism of the anisotropy of fracture characteristics. The anisotropy characteristic  $A_{KCV}$  is mainly influenced by the elongation of bcc crystals of the  $\beta$ -phase and highly dispersed precipitates of a brittle structural component ( $\alpha$ -phase) along their boundaries, similarly to the structural texture of aluminum alloy sheets examined earlier [5, 6]. For titanium alloys, with the growth of  $f_\beta$  from 50 to 100%,  $A_{KCV}$  decreases from 1 to 0.7, in the same way as  $A_{K_{1c}}$  does in aluminum alloys with an increase in  $\varepsilon$  from 0 to 0.8 (Fig. 3a).

**2.2. Comparative Analysis of Strength and Plasticity Characteristics of Titanium Alloys and Austenitic Steel at the Plane Stress State.** The specific feature of  $\alpha$ - and pseudo- $\alpha$ -titanium alloys is their texture strengthening leading to an increase in the strength of thin plates in biaxial tension as compared to the uniaxial one with a simultaneous decrease in its deformability in the direction normal to the rolling direction. The expressions  $A_{\sigma_u} = (\sigma_u)_{\sigma_1/\sigma_2=1} / (\sigma_u)_{\sigma_1/\sigma_2=\infty}$  and  $A_{\sigma_Y} = (\sigma_Y)_{\sigma_1/\sigma_2=1} / (\sigma_Y)_{\sigma_1/\sigma_2=\infty}$ , describing the ratios of the ultimate strength  $\sigma_u$  and yield stress  $\sigma_Y$  of a U-notched flat specimen in symmetrical biaxial tension ( $\sigma_1/\sigma_2 = 1$ ) to those of the standard specimen in uniaxial tension ( $\sigma_1/\sigma_2 = \infty$ ) were taken as strength anisotropy characteristics in [3, 4]. Normal plastic anisotropy was estimated by  $r = \log(b_0/b_f) / \log(h_0/h_f)$ , where  $b_0$  and  $b_f$ ,  $h_0$  and  $h_f$  are the initial and final width and thickness of the specimen. With the perfect basic texture of central type II (Fig. 2d),  $r = \infty$ , for a pure isotropic material,  $r = 1$ , under real rolling conditions of hcp metals,  $1 < r < \infty$  [4].

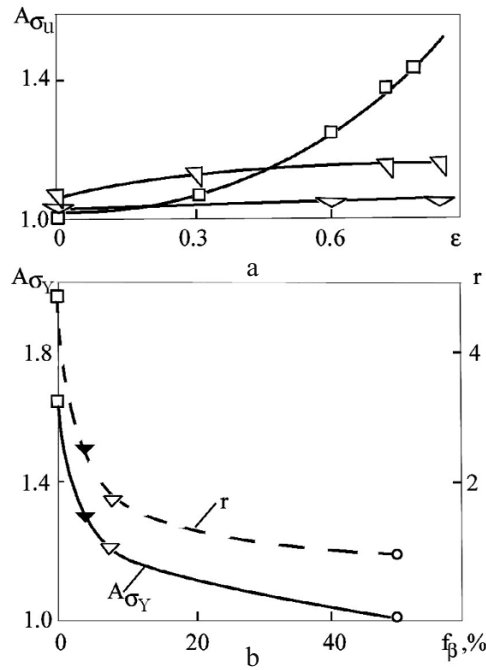


Fig. 4. Texture strengthening characteristics  $A_{\sigma_u}$ ,  $A_{\sigma_y}$  and plastic anisotropy  $r$  of titanium alloys vs strain  $\epsilon$  on rolling (a) and  $\beta$ -phase content at  $\epsilon = 0.8$  (b). (Symbols for alloys in Fig. 1 and Table 1).

2.2.1. An enhancement of strength characteristics in symmetrical biaxial tension of thin plates of  $\alpha$ - and pseudo- $\alpha$ -titanium alloys is controlled by the crystallographic  $\alpha$ -phase texture. At the plane stress state, their basic plane (0001) is directed parallel to the rolling plane by the above mechanism. With this, slip deformation of the material across its thickness becomes difficult, which determines high values of normal plastic anisotropy, compression strength, and significant strengthening in biaxial tension.

The variation of strength and plastic anisotropy characteristics in going from  $\alpha$ - and pseudo- $\alpha$ -alloys to  $(\alpha + \beta)$ -, intermediate-structure, and pseudo- $\beta$ -alloys with the growth of the initial  $\beta$ -phase content can be followed from the data in Fig. 4 with VT5-1, OT4-1, VT6, VT14, VT22, and VT15 alloys (Table 1, Fig. 1). As is seen in Fig. 4a, with an increase in the plastic strain  $\epsilon$  to 0.8, the texture strengthening characteristic  $A_{\sigma_u}$  is at its maximum for a VT5-1  $\alpha$ -alloy, then it exhibits a gradual decrease with a decrease in the  $\alpha$ -phase content to the point of its disappearance for a VT14  $(\alpha + \beta)$ -alloy and a VT15 pseudo- $\beta$ -alloy, reaching the value typical of the invariant one under a stress state for the latter ( $A_{\sigma_u} \cong 1$ ). In Fig. 4b, the variation of the strength ( $A_{\sigma_y}$ ) and plastic ( $r$ ) anisotropy with an increase in  $f_{\beta}$  is demonstrated with thin plates ( $\approx 2$  mm) from the above materials. A reduction in  $A_{\sigma_y}$  and  $r$  is most intensive over the range of  $f_{\beta} = 0-15\%$ , then they decrease monotonically, to the point of formation of intermediate-structure and pseudo- $\beta$ -titanium alloys insensitive to a stress state at  $f_{\beta} \geq 50\%$ .

2.2.2. The difference of hcp metals from the bcc and fcc ones lies in the fact that for the latter across-the-thickness strain of thin plates, mainly enhancing the structural changes in the material [7], is the necessary condition of plastic flow at the plane stress state. It has been demonstrated with thin-walled tubular specimens from 12Kh18N10T austenitic steel, plastically deformed in uniaxial ( $\sigma_z/\sigma_{\theta} = \infty$ ) and equiaxial ( $\sigma_z/\sigma_{\theta} = 1$ ) tension after cold rolling and normalization (Fig. 5a) that the maximum contribution of the radial compression component  $\epsilon_r$  to the plastic strain intensity  $\epsilon_i$  is reached at  $\sigma_z/\sigma_{\theta} = 1$  with simultaneous realizing the hypothesis for the unified deformation curve  $\sigma_i - \epsilon_i$  without pronounced texture strengthening of the material [7, 8]. Here  $\sigma_i = \sigma_i(\sigma_z, \sigma_{\theta}, \sigma_r)$  and  $\epsilon_i = \epsilon_i(\epsilon_z, \epsilon_{\theta}, \epsilon_r)$  are the intensities of stresses and strains,  $z$ ,  $\theta$ , and  $r$  correspond to the axial, tangential, and radial components of stresses and strains [8, 9].

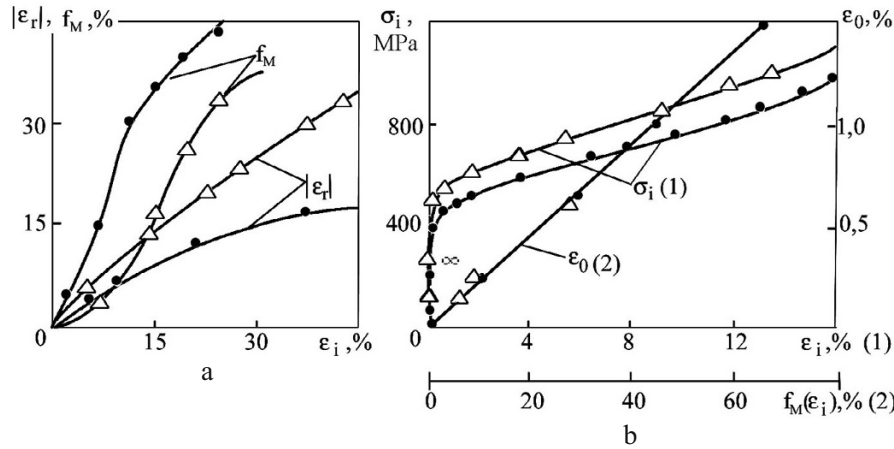


Fig. 5. Mechanical and structural characteristics of thin-walled tubular specimens from 12Kh18N10T metastable steel vs plastic strain intensity  $\epsilon_i$  at  $\sigma_z/\sigma_\theta = \infty$  (●) and 1 (△).

An enhanced function of  $\epsilon_r$  in the strain hardening of steel in biaxial tension as compared to uniaxial one is confirmed by the complexity of the dislocation structure of austenite typical of the compression process [7, 8, 10] and the retardation of strain-induced martensite formation at  $-160^\circ\text{C}$ , corresponding to the evolution of phase instability of the above steel (Fig. 5a). In this case, the mechanical behavior of steel, deformed at  $20^\circ\text{C}$ , is changed with the origin of the stable austenitic structure: the plasticity hypotheses for the unified deformation curve and elastic variation of the material volume are violated (Fig. 5b).

Wider variations of the flow stress intensity  $\sigma_i(\epsilon_i)$  of metastable austenitic steel in equiaxial tension as compared to uniaxial one (Fig. 5b, curves 1 and 2) are the result of increasing the plastic deformation resistance of initial austenitic and forming martensitic phases, induced by the growth of density of their structural defects.

Residual variations of the volume of metastable austenitic steel are illustrated with the unified linear relation between the relative volume variation, characterized by the mean plastic strain  $\epsilon_0 = 1/3(\epsilon_z + \epsilon_\theta + \epsilon_r)$ , and strain-induced martensite volume  $f_M(\epsilon_i)$  for different ratios of principal stress components  $\sigma_z/\sigma_\theta$  (Fig. 5b, curve 2) [8–10]. The growth of  $\epsilon_0$  with  $f_M(\epsilon_i)$  is determined by the larger specific volume of martensite, formed at the phase transition, than that of the initial austenite phase, which brings about the retardation of martensite transformation under a prevailing effect of the compression strain component  $\epsilon_r$  on  $\epsilon_i$ , which is typical of equiaxial tension (Fig. 5a) and compression [8].

Inherent in  $\alpha$ -, pseudo- $\alpha$ -, and  $(\alpha + \beta)$ -titanium alloys, the impediment of across-the-thickness deformation of thin plates by slipping with the perfection of the crystallographic texture of central type, ensuring texture strengthening at the plane stress state as well as the growth of the density of structural defects in metastable austenitic steel, can lead to the nonfulfillment of the hypothesis for the unified deformation curve (especially at  $0 \leq f_\beta < 15\%$ ). The latter should be considered in the strength calculations for thin-walled shell structure elements from those alloys.

The analytical description of the plastic state of an anisotropic material and the plastic zone near the crack tip with regard to the features of the hcp lattice and the stress state in the context of deformable solid body mechanics is covered in detail in [14–17].

## CONCLUSIONS

1. Investigation results are generalized and systematized to follow the effect of the crystallographic sheet texture and the structure of  $\alpha$ -, pseudo- $\alpha$ -,  $(\alpha + \beta)$ -, and pseudo- $\beta$ -titanium alloys with a gradual increase in the initial  $\beta$ -phase content on the formation patterns of anisotropy of strength and fracture resistance characteristics in relation to in-production strain levels, loading methods and directions, and mode I crack propagation.

2. The anisotropy of mechanical properties on combined and separate texture and structure strengthening was compared with the results, obtained earlier for  $\alpha$ -titanium and aluminum alloys as well as metastable austenitic steel.



3. Consideration is given to a competing effect of the crystallographic and structural sheet texture of the  $\alpha$ - and  $\beta$ -phases of thin plates from titanium alloys on a decrease in the reverse anisotropy characteristic  $A_{KCV}$  with  $f_\beta$  from 0 to 100%.

4. The  $f_\beta$  growth was demonstrated to have the effect on a decrease in the texture strengthening characteristics  $A_{\sigma_u}$ ,  $A_{\sigma_y}$  and the normal plastic anisotropy  $r$  in biaxial tension of thin plates from titanium alloys, associated with a decrease in the  $\alpha$ -phase content, which features maximum efficiency of realizing the texture preconditions for plastic strain retardation across the sheet thickness.

5. Analogy is suggested between the mechanical behavior of titanium alloys at  $f_\beta = 0$ –15% and metastable austenitic steel by the criterion of similar strain hardening in biaxial tension as a result of evolution and perfection of the crystallographic  $\alpha$ -phase texture of central type on rolling and an increase in the density of structural defects in the matrix (austenitic) phase and forming strain-induced martensite.

## REFERENCES

1. S. B. Nizhnik and E. A. Dmitrieva, "Anisotropy patterns of fracture resistance characteristics stemming from a deformation texture type in structural alloys," *Strength Mater.*, **45**, No. 5, 565–573 (2013).
2. A. A. Il'in, B. A. Kolachev, and I. S. Pol'kin, *Titanium Alloys. Composition, Structure, Properties* [in Russian], VILS-MATI, Moscow (2009).
3. B. A. Drozdovskii, L. V. Prokhodtseva, and N. I. Novosil'tseva, *Fracture Toughness of Titanium Alloys* [in Russian], Metallurgiya, Moscow (1983).
4. P. G. Miklyaev and Ya. B. Fridman, *Anisotropy of Mechanical Properties of Metals* [in Russian], Metallurgiya, Moscow (1986).
5. A. A. Kaminsky and S. B. Nizhnik, "Prediction of fracture toughness anisotropy of ageing metallic materials," *Dop. NAN Ukrainy*, No. 10, 64–68 (2008).
6. A. A. Kaminsky and S. B. Nizhnik, "Anisotropy of fracture toughness of structurally inhomogeneous ageing alloys," *Int. Appl. Mech.*, **45**, No. 9, 1016–1022 (2009).
7. S. B. Nizhnik, "Structure effect on strain hardening of austenitic and martensitic-ageing steels at the plane stress state," *Metally*, No. 1, 152–158 (1992).
8. V. N. Bastun and S. B. Nizhnik, "Studies on elastoplastic deformation mechanisms of hardening metals with regard to their structure under static loading at the multiaxial stress state," *Prikl. Mekh.*, **37**, No. 10, 24–52 (2001).
9. A. A. Lebedev, B. I. Koval'chuk, F. F. Giginyak, and V. P. Lamashevskii, *Mechanical Properties of Structural Materials at the Multiaxial Stress State* [in Russian], In Jure, Kiev (2003).
10. B. I. Koval'chuk, A. A. Lebedev, and S. É. Umanskii, *Mechanics of Inelastic Deformation of Materials and Structural Elements* [in Russian], Naukova Dumka, Kiev (1987).
11. A. W. Bowen, "The influence of crystallographic orientation on the fracture toughness of strongly textured Ti–6Al–4V," *Acta Metall.*, **26**, No. 9, 1423–1433 (1978).
12. V. P. Sylovanyuk, R. Ya. Yukhym, and P. V. Horbach, "Deformation and fracture of materials near spheroidal inclusions," *Mater. Sci.*, **46**, No. 6, 757–762 (2011).
13. R. W. K. Honeycombe, *The Plastic Deformation of Metals*, Edward Arnold, London (1972).
14. Yu. N. Loginov, V. D. Solovey, and V. V. Kotov, "Transformation of the yield condition under deformation of metallic materials with the hcp lattice," *Metally*, No. 2, 93–99 (2010).
15. A. A. Kaminsky, E. E. Kurchakov, and G. V. Gavrilov, "Influence of tension along a crack on the plastic zone in an anisotropic body," *Int. Appl. Mech.*, **46**, No. 6, 634–648 (2010).
16. A. A. Kaminsky and E. E. Kurchakov, "Modeling the fracture process zone near a crack tip in a nonlinear elastic body," *Int. Appl. Mech.*, **47**, No. 6, 735–744 (2011).
17. A. A. Kaminsky and E. E. Kurchakov, "Modeling a crack with a fracture process zone in a nonlinear elastic body," *Int. Appl. Mech.*, **48**, No. 5, 552–562 (2012).